Supplementary file C

The tungsten-182 record of kimberlites above the African superplume

S. Tappe, G. Budde, A. Stracke, A. Wilson, T. Kleine

" Supplementary Information "

This file includes:

Supplementary Results / Discussion
Supplementary Figures 1-11 / Tables 1-4

Samples

A unique collection of fresh and uncontaminated magmatic kimberlite samples from 18 occurrences in sub-Saharan Africa is investigated here. The samples are derived from East Africa (Tanzania), Central Africa (Angola), and southern Africa (Namibia, Botswana, South Africa, Lesotho). This continental shield region stretches over >3,000 km from the Atlantic Ocean in the west to the Indian Ocean in the east, and it predominantly comprises Precambrian basement bedrocks. The study region is commonly referred to as the Southern African Plateau given its generally high elevation >1,000 m, as recognizable in the ETOPO-1 digital elevation model for sub-Saharan Africa (Fig. S1).

The investigated kimberlite occurrences span an age range from 1835 Ma to 0.012 Ma (Table S1)[1-13], which is representative of the age record for global kimberlite magmatism[2]. On the basis of petrography and mineralogy the samples represent aphanitic to macrocrystic coherent magmatic Group-1 kimberlites, hereafter referred to simply as 'kimberlites'. Although olivine macrocrysts and phenocrysts are commonly serpentinized, pristine olivine is present in most samples set in a fresh groundmass that typically consists of spinel, perovskite, rutile, ilmenite, phlogopite, apatite, calcite, monticellite, and primary serpentine (Fig. S2). Several southern African kimberlites have entrained diamonds with transition zone and lower mantle mineral inclusion assemblages[14]. Of the investigated kimberlite occurrences, at least five localities contain such 'ultradeep' diamonds originating from >400 km depths (e.g., Cullinan/Premier[15-17], Jagersfontein[18], Karowe Orapa A/K6[19], Monastery[20], Letseng[16]).

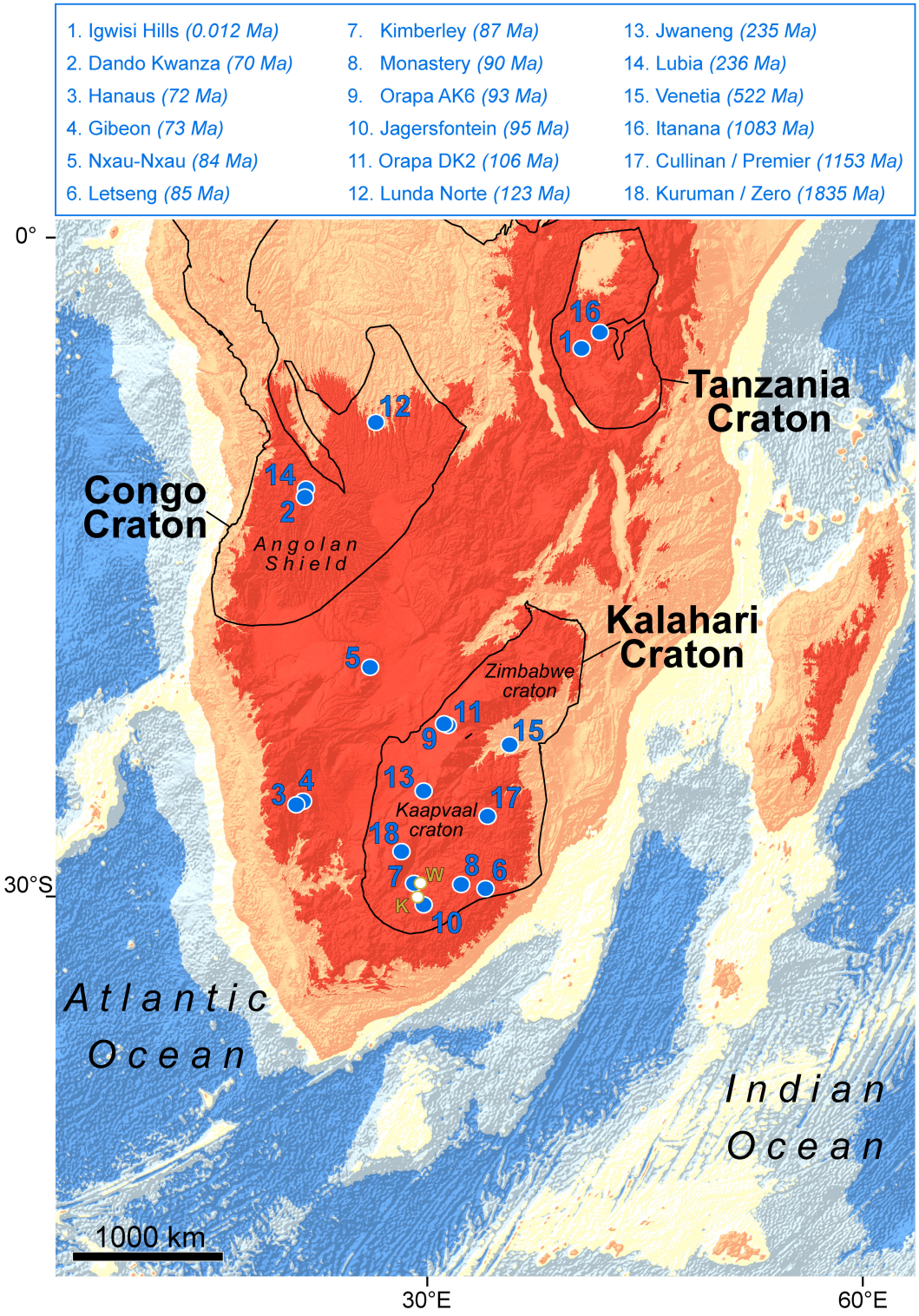

Figure S1. Sample sites for kimberlites analyzed during this tungsten-182 study. Magmatic Group-1 kimberlite sample localities in sub-Saharan Africa superimposed on the ETOPO-1 digital elevation model (Mollweide projection). The regions in red have elevations >1,000 m and the black outlines demarcate Archaean cratons *sensu stricto* (the map is modified after ref. [2]). Detailed information about the 18 kimberlite occurrences investigated here can be found in Table S1. The tungsten isotopic compositions are displayed in Figure 9 of the main text and summarized in Tables S2 and S3. The ca. 91 Ma old Wesselton ('W') and Koffiefontein ('K') kimberlite pipes on the Kaapvaal craton in South Africa have been analyzed previously for their tungsten isotopic compositions[21].

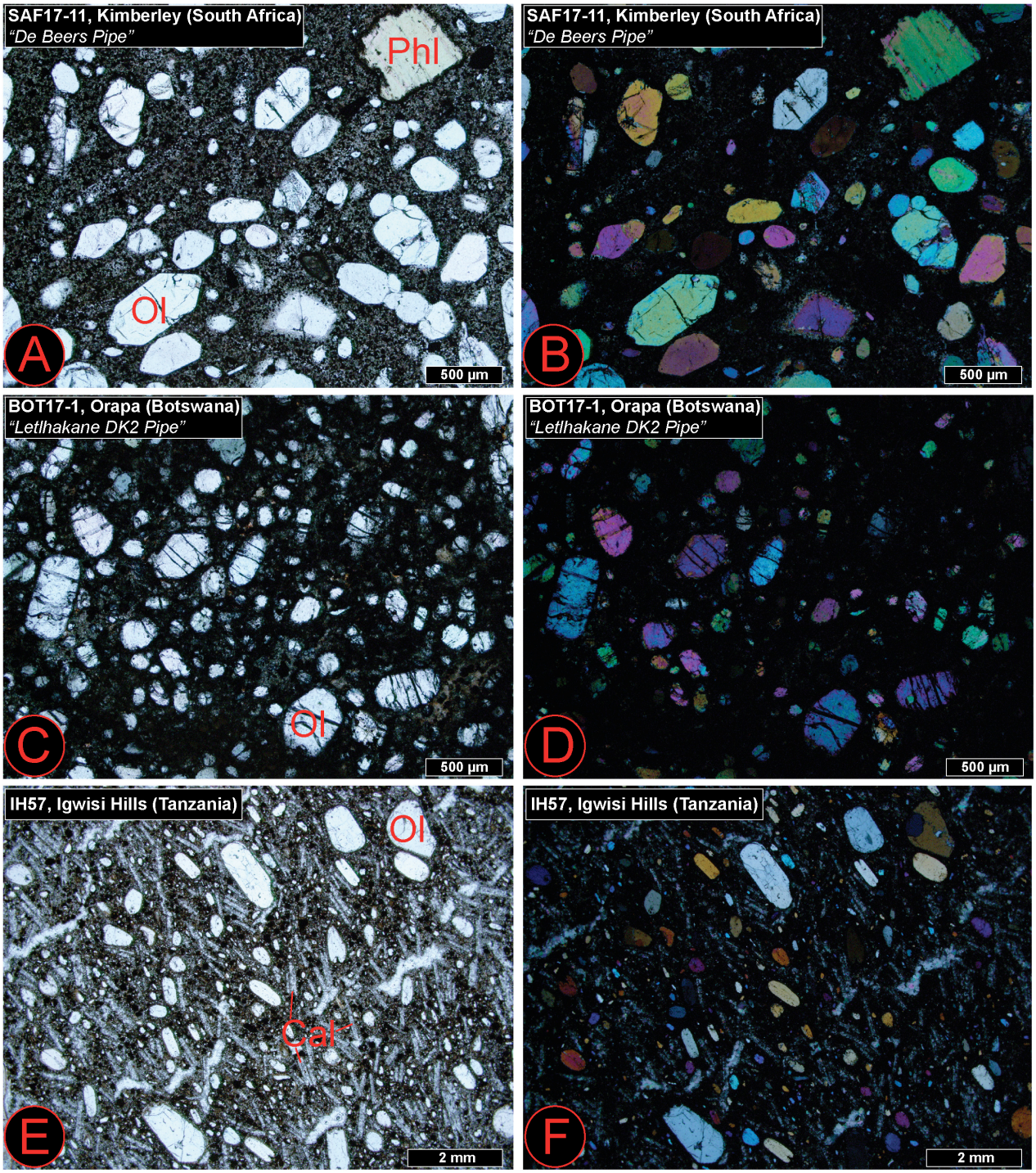

Figure S2. Photomicrographs of representative magmatic kimberlite samples from Africa. (A-B) Sample SAF17-11 from a microporphyritic kimberlite dyke ('Westhanlage Dyke', 510 m below surface) within the 'De Beers Pipe' of the Kimberley kimberlite cluster in South Africa. (C-D) Sample BOT17-1 from a microporphyritic kimberlite plug within the 'Letlhakane D/K2 Pipe' of the Orapa kimberlite field in Botswana. (E-F) Sample IH57 from a macrocrystic kimberlite lava flow of the Igwisi Hills kimberlite volcanoes in Tanzania. Note the flow-alignment of olivine and calcite crystals.
Panels A-C-E represent images taken under plane polarized light, and Panels B-D-F are the respective counterpart images taken under crossed polarized light. Ol = olivine, Phl = phlogopite, Cal = calcite.

Geochemistry

The major and trace element concentrations, as well as the Sr-Nd-Hf-C-O isotopic compositions of the magmatic kimberlite samples from the 18 sub-Saharan occurrences analyzed during this study are listed in Supplementary file B. The results for the tungsten isotope ratio measurements, as well as the Hf and W element abundance determinations by ID-MC-ICP-MS are listed in Table S2. Table S3 provides a summary of the tungsten isotopic compositions of the 18 studied kimberlite occurrences. Table S4 lists the tungsten isotope results for the reference materials analyzed during this study. The complete dataset is provided for download from the online version (Supplementary file B), and all investigated kimberlite occurrences are displayed on the digital elevation map of sub-Saharan Africa in Fig. S1.

Major and trace element compositions

The fresh kimberlite samples selected for this tungsten isotope study have major element compositions that fall firmly within the compositional range defined by magmatic Group-1 kimberlites from worldwide occurrences (Fig. S3). The sample suite has been divided into Modern, Phanerozoic, and Proterozoic kimberlite subsets; however, the relatively small number of samples analyzed precludes an assessment of whether or not there exist systematic major element differences between the age groups. The kimberlite samples have variably high MgO (17.2-34.9 wt.%), Ni (245-1361 ppm), and Cr (171-1656 ppm) concentrations. The SiO_2 (20.7-34.8 wt.%), Al_2O_3 (1.5-4.0 wt.%), and Na_2O (<0.05-0.18 wt.%) contents are generally low. Concentrations of TiO_2 (0.9-4.1 wt.%), K_2O (<0.05-2.5 wt.%), and P_2O_5 (0.13-3.8 wt.%) are highly variable but fall within the range of global Group-1 kimberlites (Fig. S3). The CaO (3.7-21.7 wt.%) and CO_2 (0.1-11.3 wt.%) contents vary widely, mainly as a function of the modal abundances of olivine crystal cargo and primary groundmass carbonate (i.e., variations along olivine and calcite control lines). The samples scatter around estimates of parental kimberlite melts from worldwide occurrences in terms of major element compositions (Fig. S3). Importantly, the Contamination Index[22] (C.I. = [SiO_2+Al_2O_3+Na_2O] / [MgO+2*K_2O]) for the studied kimberlites ranges from 0.83 to 1.39, with the majority of samples being close to unity (Fig. S3f). This observation suggests that interaction with and assimilation of granitic continental crust has been minimal or absent[23,24], which is also supported by the high values for ln Si/Al and ln Mg/Yb[24] (Supplementary file D).

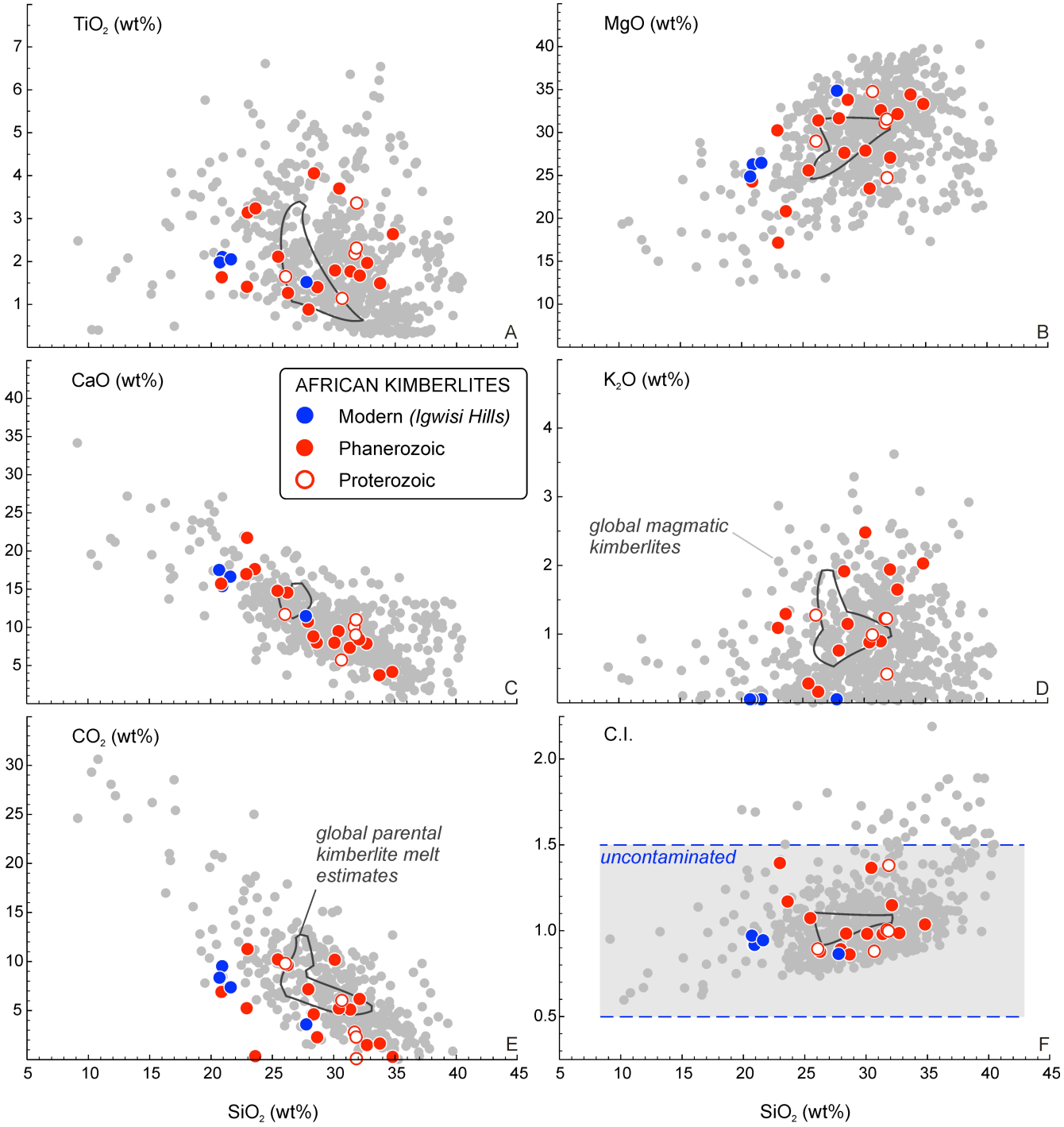

Figure S3. Kimberlite major element variation diagrams. Variation diagrams of TiO_2 (A), MgO (B), CaO (C), K_2O (D), CO_2 (E), and C.I. (F) *versus* SiO_2 (wt.%) for the African kimberlite samples studied here for their tungsten isotopic compositions. The compilation of screened high-quality data for fresh magmatic kimberlites from worldwide occurrences is taken from ref. [25]. The dark grey outlines mark the compositional space occupied by reconstructed parental kimberlite magmas from key cratons worldwide[24]. Contamination Index (C.I. = $[SiO_2+Al_2O_3+Na_2O]/[MgO+2*K_2O]$) values of 1.0 ±0.5 indicate that kimberlite magmas were not, or only minimally, contaminated with crustal basement materials upon ascent[22-24].

All sub-Saharan kimberlites investigated here are characterized by enriched incompatible trace element concentrations relative to primitive mantle. In general, the samples show similar primitive mantle normalized distributions to each other that are notably more fractionated (i.e., pronounced troughs and spikes) than the patterns of incompatible element enriched OIBs from the South Atlantic[26] (Fig. S4). For most samples, the Ba, Th, U, Nb, Ta, La, and Ce concentrations exceed 100 times primitive mantle values, and relative depletions occur at K, Pb, Zr-Hf, and the HREE (Fig. S4). A peculiar feature of the recent Igwisi Hills kimberlite lavas from the Tanzania craton is the strong Cs-Rb depletion (Fig. S4a), which is coupled to extremely low K contents at around the 0.05 wt.% K_2O detection limit of the XRF method. The kimberlite lavas from Dando Kwanza (ANG14-325) and Gibeon (NAM18-02) on the Angolan Shield and Kalahari craton, respectively, also show pronounced depletions in Cs-Rb-K (Fig. S4b). This geochemical signature reflects the original low modal abundance or absence of phlogopite in these particular extrusive kimberlites rather than large-ion lithophile element mobility due to alteration. The Gibeon kimberlite sample NAM18-02 is characterized by an exceptionally high tungsten content (21.8 ppm), which cannot be related readily to interaction with the regional metamorphic crust of the Rehoboth block in Namibia (see below). The magmatic kimberlite sample BOT17-05 from the Jwaneng kimberlite cluster on the western Kaapvaal craton exhibits subtle relative depletions in Nb-Ta, which is more typical for Group-2 kimberlites[27,28]. The subtle Group-2 kimberlite trace element signature of the Jwaneng kimberlite is also apparent from its elevated Th/Nb, Ba/Nb, and La/Nb ratios (Fig. S5), which are primarily a consequence of the Nb depletion. Furthermore, the low Ce/Pb ratio observed in Fig. S6 is also an indication of involvement of metasomatized cratonic mantle lithosphere in the genesis of the Jwaneng kimberlite magma, as typically envisaged for Group-2 kimberlite magma formation[27]. Samples SAF18-58 and SAF18-59 from Zero pipe of the Proterozoic Kuruman kimberlite field at the western Kaapvaal craton margin show exceptionally high Th concentrations reaching 57.5 ppm, which results in very high Th/Nb ratios similar to Group-2 kimberlites (Fig. S5a). However, this geochemical signature is not due to Nb depletion, as in the case of Group-2 kimberlites, but it merely reflects the strong Th and LREE enrichment of the Zero kimberlite (Figs. S5, S6). The majority of sub-Saharan kimberlite samples have similar Th/Nb, Ba/Nb, La/Nb, and Ce/Pb ratios falling within the compositional range known for archetypal Group-1 kimberlites from South Africa[23] (Figs. S5, S6). For these incompatible element concentration ratios there also exists significant overlap between African kimberlites and South Atlantic OIBs, as first noted by ref. [29].

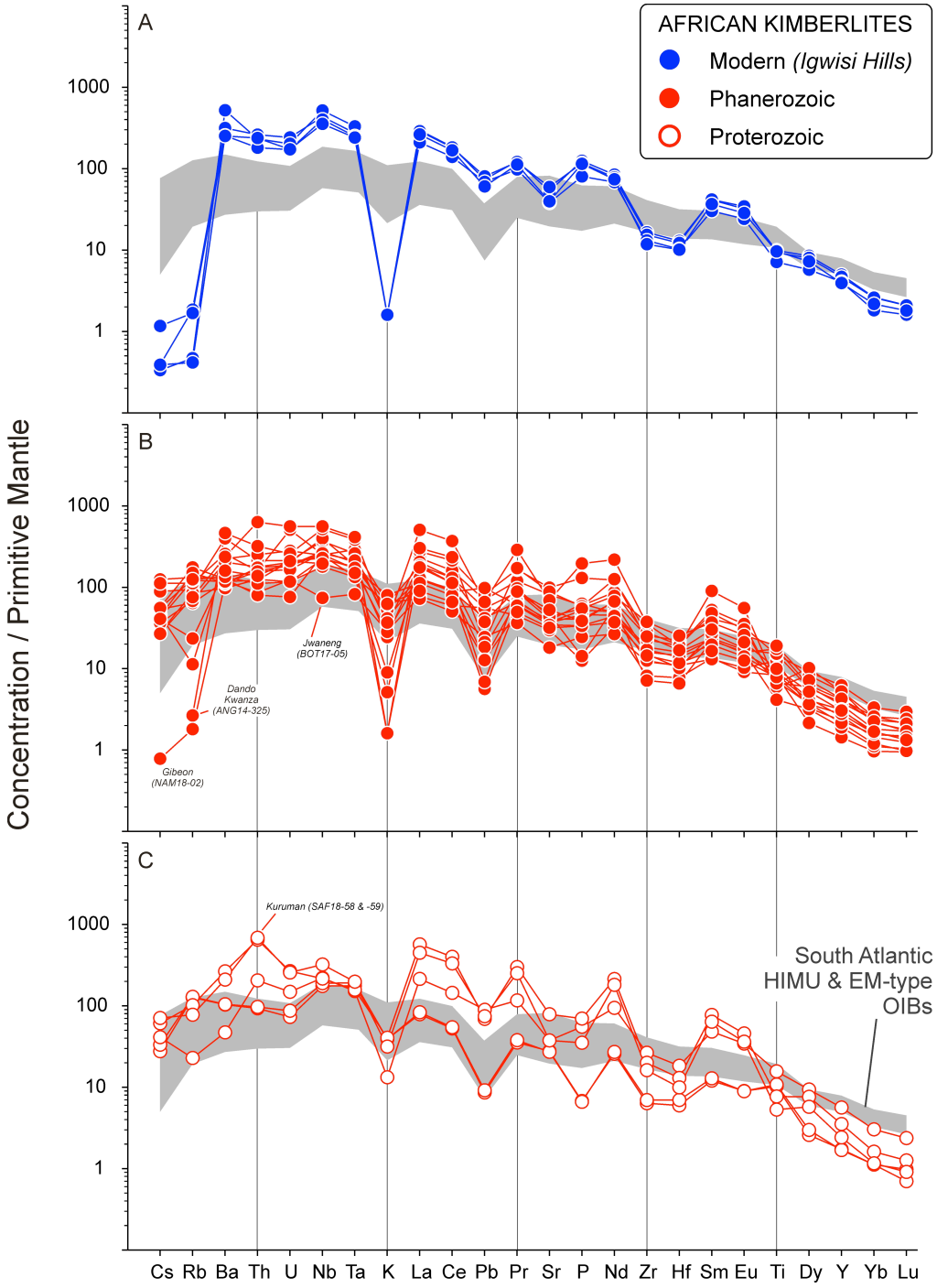

Figure S4. Kimberlite trace element distribution patterns. Primitive mantle normalized incompatible element distributions for the African kimberlite samples. The dataset has been divided into (A) 'Modern' kimberlite represented by the Igwisi Hills occurrence on the Tanzania craton, (B) 'Phanerozoic' kimberlites ranging in age from 522 Ma to 70 Ma, and (C) 'Proterozoic' kimberlites ranging in age from 1835 Ma to 1083 Ma (see Table S1). The grey field displayed for comparison in all panels comprises incompatible element patterns for HIMU-type (St. Helena) and EM-type (Tristan and Gough) OIBs from the South Atlantic[26]. Primitive mantle element concentrations are from ref. [30].

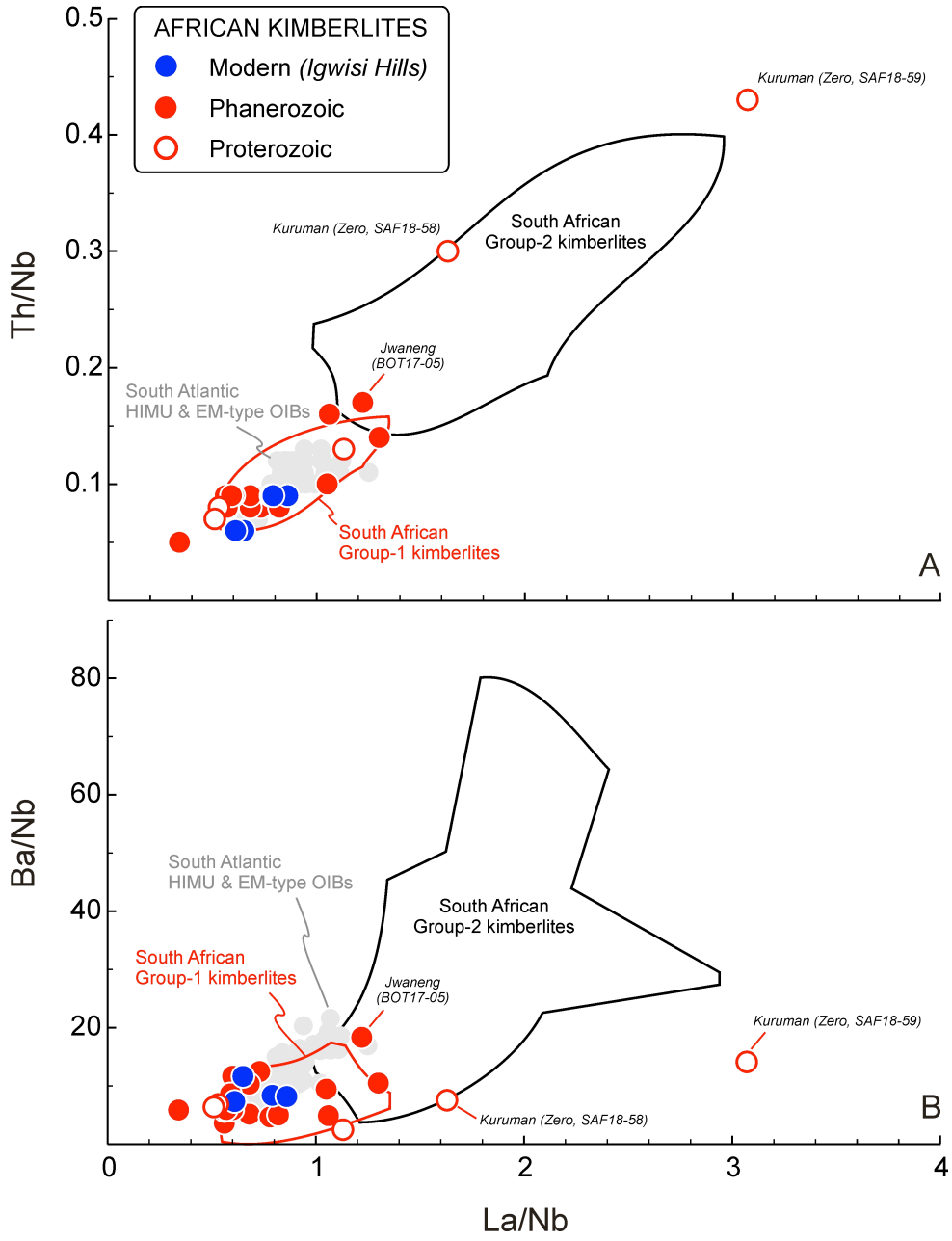

Figure S5. Trace element ratio variation diagrams for African kimberlites. Incompatible element concentration ratio variation diagrams for the kimberlite samples from sub-Saharan Africa. (A) The Th/Nb versus La/Nb systematics show the general Group-1 kimberlite character of the samples, but it is noted that the two Kuruman kimberlite samples from Zero pipe (SAF18-58 and SAF18-59) show strong Th and La enrichment resulting in very high Th/Nb and La/Nb, which is more typical for Group-2 kimberlites, albeit due to relative depletions in Nb. Note further the slightly elevated Th/Nb and La/Nb ratios of the Jwaneng kimberlite sample BOT17-05 (caused by a relative Nb depletion), placing this material into the Group-2 kimberlite field. (B) The Ba/Nb versus La/Nb systematics confirm the Group-2 kimberlite incompatible trace element character of the Jwaneng sample BOT17-05. The pronounced data overlap between sub-Saharan kimberlites and South Atlantic OIBs, as observed in both Panel A and B, was originally described by ref. [29]. Data field for South African Group-1 kimberlites is based on analyses by refs. [23,27]. Data field for South African Group-2 kimberlites is based on analyses by refs. [27,28]. Data for HIMU-type (St. Helena) and EM-type (Tristan and Gough) OIBs from the South Atlantic are shown as grey circles[26].

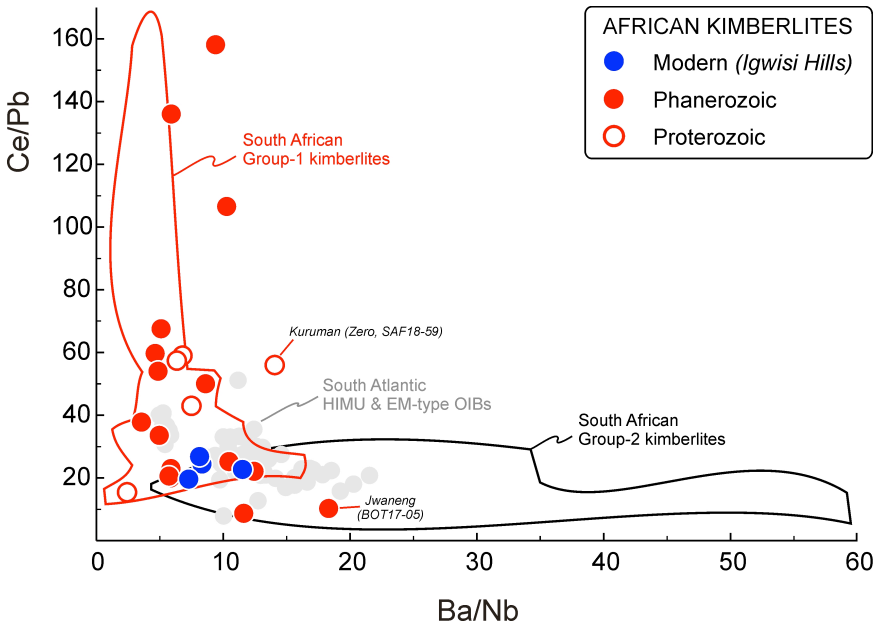

Figure S6. Ce/Pb and Ba/Nb variation diagram for African kimberlites. Incompatible element concentration ratio of Ce/Pb versus Ba/Nb for the kimberlite samples from sub-Saharan Africa. The majority of samples show a general Group-1 kimberlite character, with the exceptions of samples from Zero pipe at Kuruman (SAF18-59) and from Jwaneng (BOT17-05), which are relatively enriched in Ba or depleted in Nb, as is more typical for Group-2 kimberlites. Data field for South African Group-1 kimberlites is based on analyses by refs. [23,27]. Data field for South African Group-2 kimberlites is shown for discussion purposes and based on analyses by refs. [27,28]. Data for HIMU-type (St. Helena) and EM-type (Tristan and Gough) OIBs from the South Atlantic are shown as grey circles[26].

The sample suite of sub-Saharan kimberlites displays a wide range of tungsten concentrations between 164 ppb and 8 ppm (NAM18-02 with 21.8 ppm W as an outlier; see below). The lower and middle parts of this range overlap with the tungsten concentrations of OIBs and continental mafic potassic lavas from worldwide occurrences (Fig. S7). The W/Th and W/U ratios of the kimberlite sample suite show weak positive correlations with the tungsten elemental abundances. These ratios of similarly incompatible elements in the bulk silicate Earth system fall largely within the modern mantle range[31]. However, a few kimberlite samples at the lower and upper end of the tungsten concentration range deviate slightly from W/Th and W/U mantle values (Fig. S7), which is best ascribed to local fractionation effects caused by accumulation and removal of accessory groundmass phases such as $CaTiO_3$-perovskite and rutile. It must be noted, however, that the studied Proterozoic to recent sub-Saharan kimberlites correspond much better to the W/Th and W/U compositions of the modern mantle than 3.5 Ga old komatiite lavas from the Kaapvaal craton in South Africa (Fig. S7). These komatiites have significantly elevated W/Th and W/U ratios[32,33].

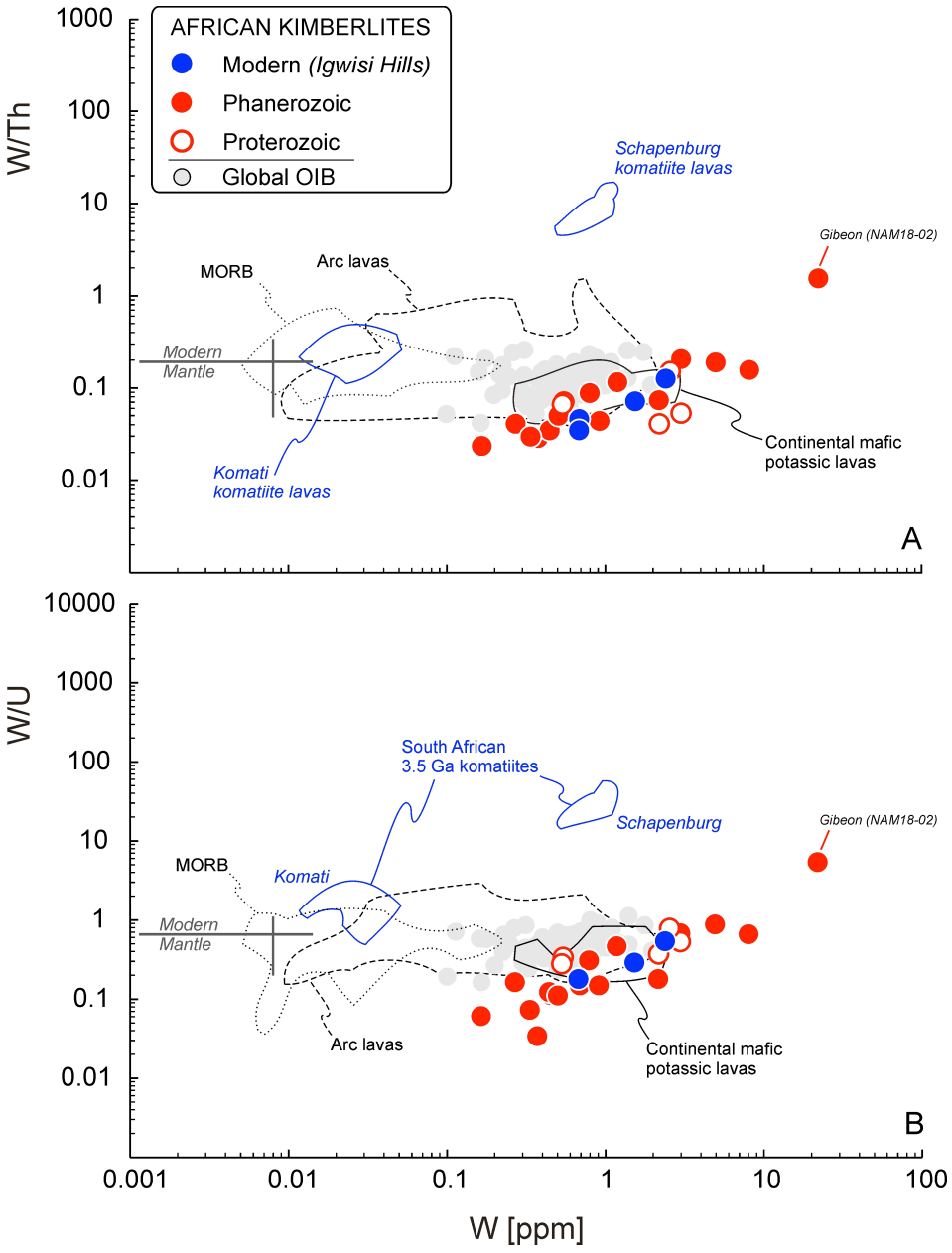

Figure S7. W/Th and W/U versus tungsten abundances of African kimberlites. Incompatible element concentration ratios of (A) W/Th and (B) W/U versus tungsten concentrations (ppm) for the kimberlite samples from sub-Saharan Africa. The kimberlite sample suite exhibits a tungsten concentration range over 2-orders of magnitude overlapping with mafic alkaline lavas from oceanic (e.g., OIBs) and continental (e.g., East African Rift) intraplate settings. The strong tungsten enrichment of sample NAM18-02 from the Gibeon kimberlite field in Namibia appears to be caused by a groundmass rutile nugget effect. The W/Th and W/U ratios of magmatic kimberlites from sub-Saharan Africa show more variability compared with primitive volcanic rocks from modern oceanic (MORB and OIB) and continental (convergent plate margin and rift) settings. However, the W/Th and W/U values for kimberlites are less extreme than those for Early Archaean komatiites from the Kaapvaal craton in South Africa. Data fields for MORB, OIB, and primitive arc plus continental rift volcanic rocks are based on analyses by refs. [26,31,34-36]. Data fields for the ca. 3.5 Ga old komatiites from the Barberton (Komati Formation) and Schapenburg supracrustal belts on the Kaapvaal craton in South Africa are based on analyses by refs. [32,33]. The compositional range for the modern Earth's mantle is adopted from ref. [31].

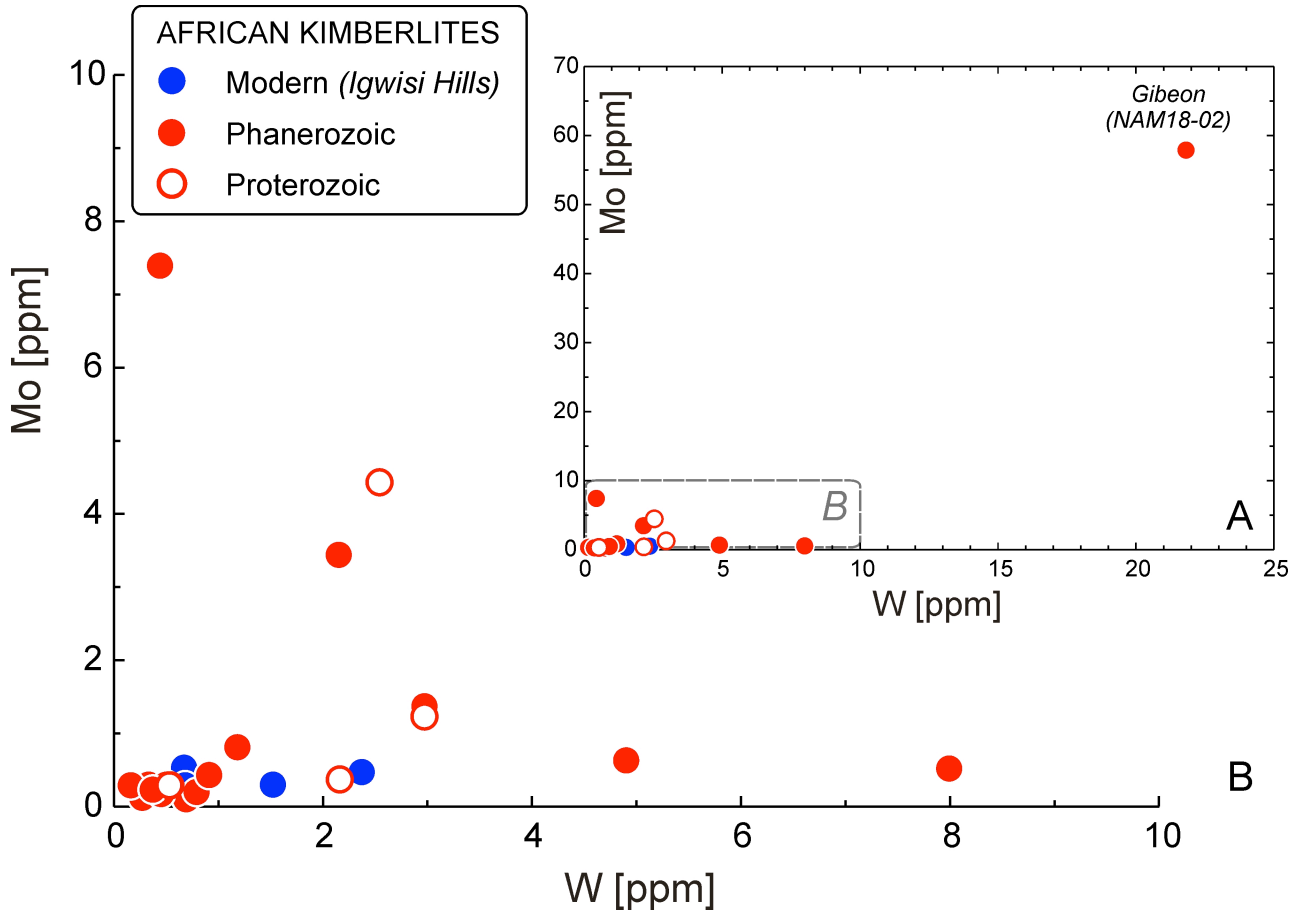

Figure S8. Molybdenum and tungsten abundances of African kimberlites. (A-B) Molybdenum versus tungsten concentrations (ppm) for the kimberlite samples from sub-Saharan Africa. Panel A provides an overview of the entire concentration range observed during this study, and Panel B shows more detail of the element variations below 10 ppm. The high molybdenum and tungsten concentrations of Gibeon kimberlite sample NAM18-02 from Namibia are due to abundant groundmass rutile.

The observed high tungsten concentrations for a few kimberlite samples are unlikely to be caused by contamination with steel equipment during rock processing, because sample exposure to steel tools was avoided (see Supplementary file A). Any potential sample contamination with steel can be excluded provided that elevated tungsten abundances >2 ppm do not correlate with molybdenum concentrations (Fig. S8). Molybdenum is an additional element typically used in steel manufacturing. Elevated tungsten concentrations at the lower ppm-level are expected for low-degree mantle-derived melts such as kimberlites (Fig. S9), given its highly incompatible nature in silicate systems similar to that of thorium and uranium[31]. An origin of tungsten in our kimberlite samples from crustal fluids can be ruled out based on mantle-like W/Th and W/U values (Fig. S7), and the fact that Archaean cratonic crust

(host to kimberlite intrusions) is predominately composed of granitoid plutons and ultramafic supracrustal rocks that typically have anomalous $^{182}W/^{184}W$ (e.g., refs. [37,38]), which is not observed for the African kimberlites studied here (see main text; average $\mu^{182}W$ value of 0.0 ± 3.9 for 18 occurrences).

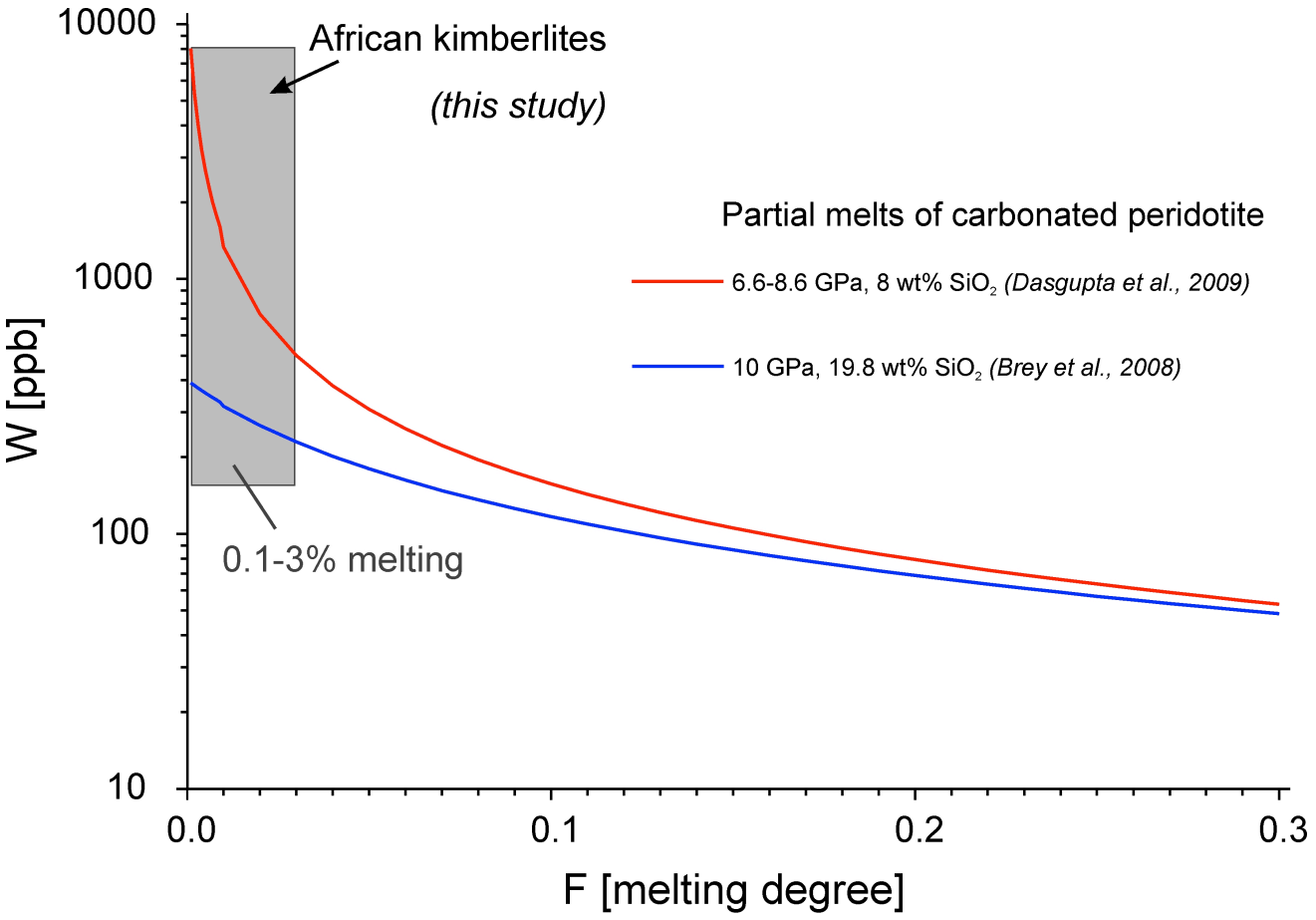

Figure S9. Melting model of peridotite to constrain the tungsten abundances of African kimberlites. The evolution of tungsten abundances (ppb) during changing degrees of batch partial melting (F) of garnet-bearing peridotite in the presence of CO_2 under upper mantle conditions (equivalent to ~200-300 km depths) is shown by the blue and red curves. The tungsten content of a fertile peridotite source was set at 16 ppb, which is equivalent to the primitive mantle value[30]. The tungsten concentration range of pristine magmatic kimberlites analyzed during this study (excluding NAM18-02) is shown as grey field. The bulk peridotite / kimberlite-carbonatite melt partition coefficients K_D for tungsten are those determined for uranium (as a proxy) in the high-pressure experimental studies of ref. [39] (0.04) and ref. [40] (0.001). Using uranium as a proxy for tungsten is justified on the basis of the identical incompatibility of these two elements in metal-free silicate-dominated systems[31]. The results demonstrate that lower ppm-level tungsten enrichment is readily achieved during near-solidus partial melting (0.1-3%) of volatile-fluxed ambient upper mantle beneath cratons.

Sr-Nd-Hf isotopic compositions

The sub-Saharan kimberlite samples fall firmly within the Sr-Nd (Fig. S10) and Nd-Hf (Fig. S11) isotope mantle arrays defined by modern MORB and OIB, with the exception of the Jwaneng sample BOT17-05, which shows Sr-Nd-Hf isotopic enrichment (see below). The initial $^{87}Sr/^{86}Sr$ ratios of most kimberlite samples range from 0.70313 to 0.70535. The initial $^{143}Nd/^{144}Nd$ ratios are superchondritic, with a narrow range of $\varepsilon_{Nd(i)}$ values between +0.3 and +4.3. In contrast, the initial $^{176}Hf/^{177}Hf$ ratios show a much wider range, with $\varepsilon_{Hf(i)}$ values between -7.2 and +9.3. These moderately depleted to slightly enriched Sr-Nd-Hf isotopic compositions are characteristic for magmatic Group-1 kimberlites from southern Africa and worldwide occurrences (Figs. S10, S11). By comparison, the Jwaneng sample BOT17-05 has notably more enriched isotopic compositions ($^{87}Sr/^{86}Sr_i = 0.70784$; $\varepsilon_{Nd(i)} = -6.1$; $\varepsilon_{Hf(i)} = -2.0$), similar to Group-2 kimberlites from the Kaapvaal craton in South Africa (Figs. S10, S11).

Although the majority of sub-Saharan kimberlites analyzed here fall within the Nd-Hf isotope mantle array (defined by $\Delta\varepsilon_{Hf}$ values between -5 and +5; where initial $\Delta\varepsilon_{Hf} = \varepsilon_{Hf(i)} - [1.59* \varepsilon_{Nd(i)} + 1.28]$), most samples plot below the terrestrial Nd-Hf isotope regression line[41] and have by definition negative initial $\Delta\varepsilon_{Hf}$ values, with the most extreme $\Delta\varepsilon_{Hf}$ value of -11.8 for the Venetia kimberlite sample SAF17-15 (Fig. S11). This observation is in good agreement with a previous combined Nd-Hf isotope study of southern African Group-1 kimberlites[42], and several subsequent studies on kimberlites from Greenland[25,43,44], North America[45-47], Asia[48,49], and Antarctica[50] established that decoupled Nd-Hf isotope systematics are a common feature of magmatic kimberlites worldwide.

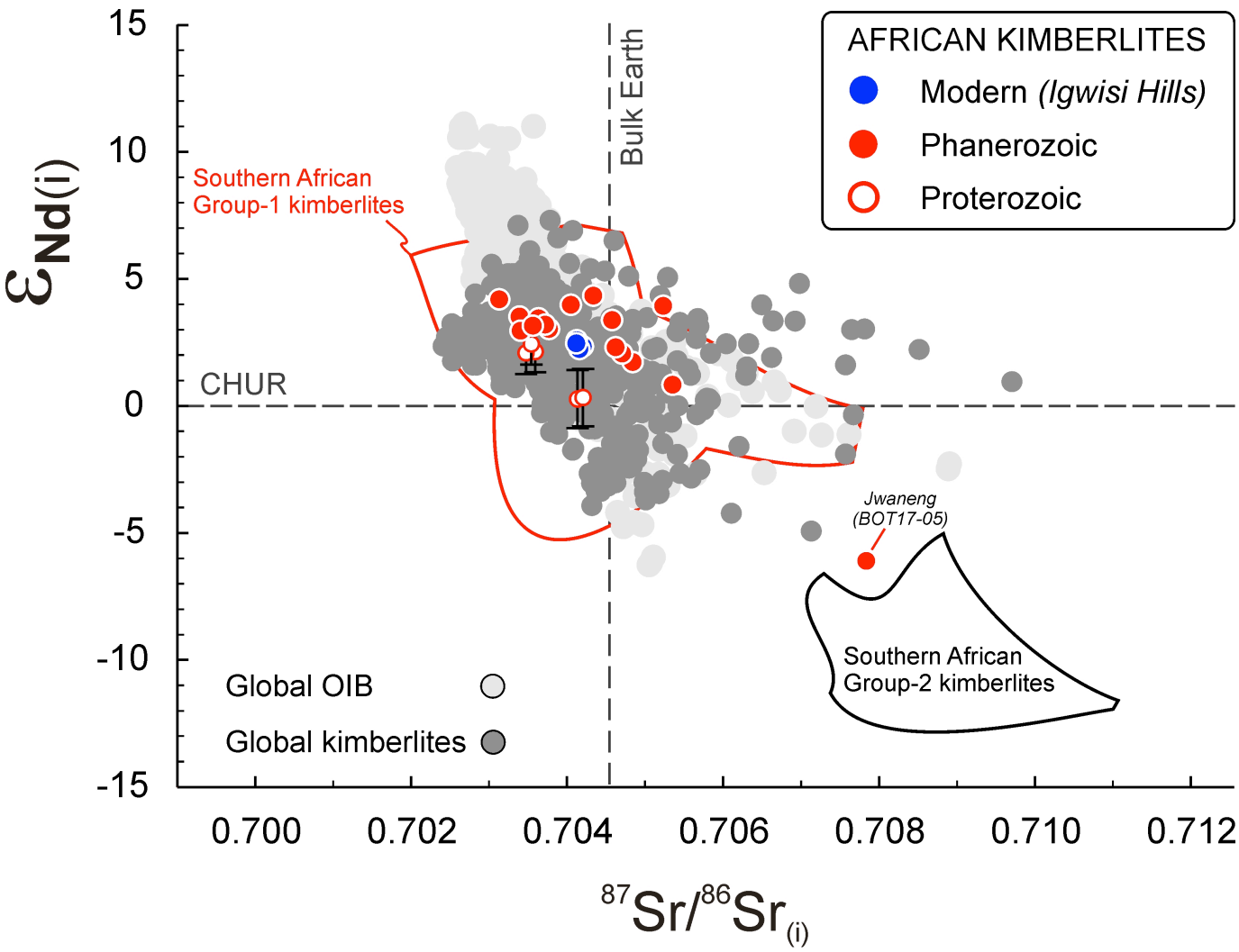

Figure S10. Neodymium and strontium isotopic compositions of African kimberlites. Initial εNd *versus* $^{87}Sr/^{86}Sr_{(i)}$ compositions of the African kimberlite samples studied here. Uncertainties are smaller than or similar to symbol size except in cases where error bars are displayed, the lengths of which entail a full propagation of uncertainties (see Methods). The compilation of Sr-Nd isotope data for global magmatic Group-1 kimberlites comprises both bulk rock and groundmass perovskite analyses[25]. Data field for Southern African Group-1 kimberlites is shown separately and based mainly on analyses by refs. [7,42,51,52]. Data field for Southern African Group-2 kimberlites is shown for discussion purposes[28,42]. The compilation of data for modern OIBs was retrieved from http://georoc.mpch-mainz.gwdg.de/georoc.

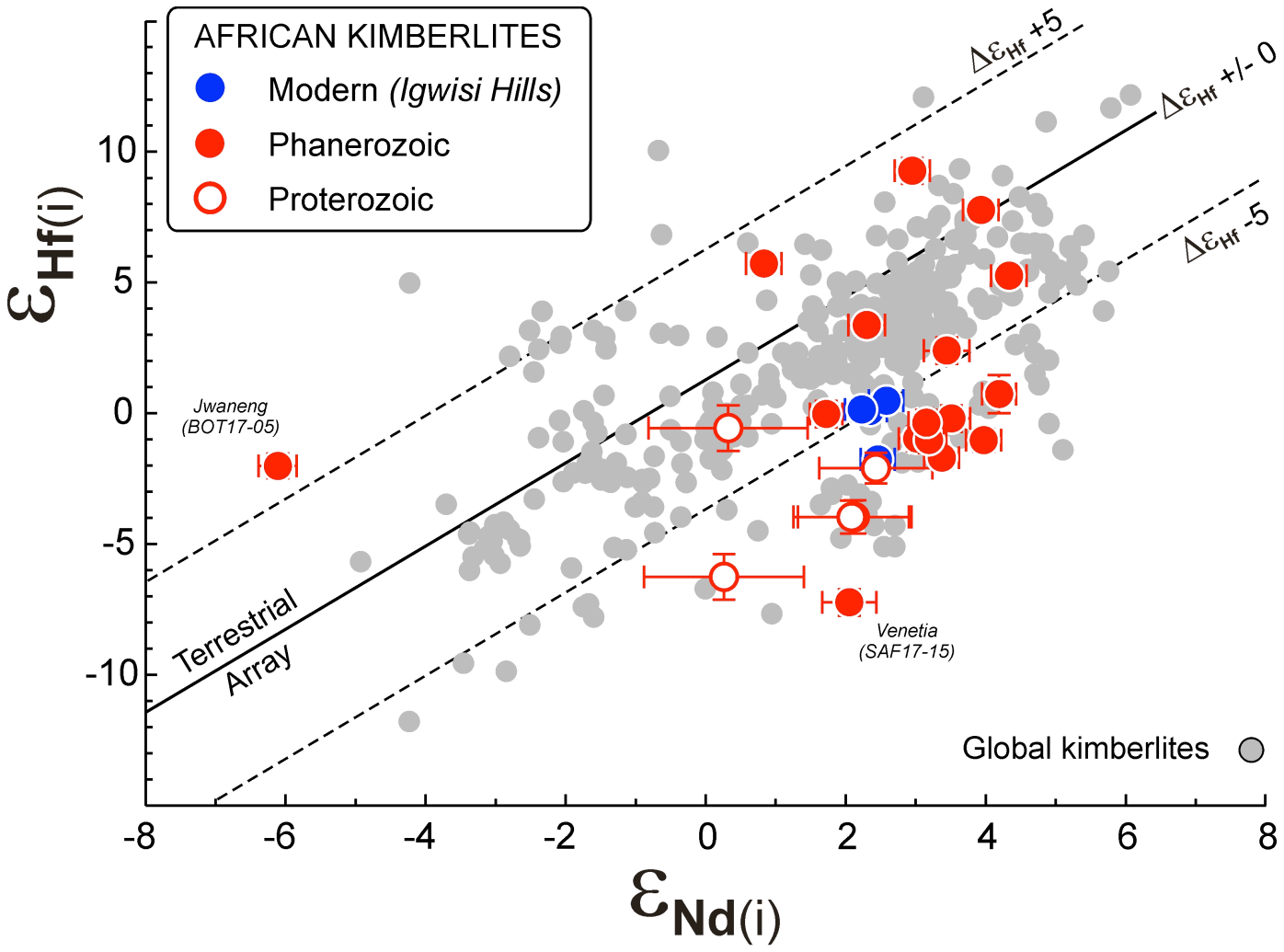

Figure S11. Hafnium and neodymium isotopic compositions of African kimberlites. Initial εHf *versus* $\varepsilon Nd_{(i)}$ compositions of the African kimberlite samples studied here. The displayed error bars entail a full propagation of uncertainties (see Methods). The data compilation of Nd-Hf isotopic compositions for global magmatic Group-1 kimberlites is taken from ref. [25]. The terrestrial array (regression line of $\Delta\varepsilon_{Hf} = 0$) is adopted from ref. [41].

Table S1: Summary of Group-1 kimberlite samples from sub-Saharan Africa investigated during this tungsten-182 study (sorted by emplacement age).

Sample ID:	Run ID:	Locality:	Country:	Age [Ma]:	Uncertainty: [Ma, 2SD]	Age Method:	Age Reference:		[a]Latitude:	[a]Longitude:
MODERN										
IH17	K12	Igwisi Hills	Tanzania	0.012	0.004	He-in-ol	Brown et al. (2012)	[1]	-4.86670	31.91670
IH45	K28	Igwisi Hills	Tanzania	0.012	0.004	He-in-ol	Brown et al. (2012)	[1]	-4.86670	31.91670
IH53	K13	Igwisi Hills	Tanzania	0.012	0.004	He-in-ol	Brown et al. (2012)	[1]	-4.86670	31.91670
IH57	K7	Igwisi Hills	Tanzania	0.012	0.004	He-in-ol	Brown et al. (2012)	[1]	-4.86670	31.91670
PHANEROZOIC										
ANG14-325	K16	Dando Kwanza	Angola	70	1	U/Pb bdl	Tappe et al. (2018a)	[2]	-11.35651	17.01033
NAM18-01	K29	Hanaus	Namibia	72	1	Rb/Sr phl	Tappe et al. (2018a)	[2]	-25.23920	17.70890
NAM18-02	K18	Gibeon	Namibia	73	8	Rb/Sr phl	Tappe et al. (2018a)	[2]	-24.99310	17.80110
BOT17-09	K3	Nxau-Nxau (K29 Pipe)	Botswana	84	4	U/Pb prv	Farr et al. (2018)	[3]	-18.94705	21.14181
LES17-01	K23	Letseng (Main Pipe)	Lesotho	85.5	0.3	U/Pb prv	Stamm et al. (2018)	[4]	-29.00600	28.86700
LES17-02	K8	Letseng (Main Pipe)	Lesotho	85.5	0.3	U/Pb prv	Stamm et al. (2018)	[4]	-29.00600	28.86700
LES17-03	K24	Letseng (Main Pipe)	Lesotho	85.5	0.3	U/Pb prv	Stamm et al. (2018)	[4]	-29.00600	28.86700
SAF17-11	K9	Kimberley (De Beers Pipe)	South Africa	87	4	U/Pb prv	Batumike et al. (2008)	[5]	-28.73890	24.77640
SAF18-57	K20	Monastery	South Africa	89.8	0.3	U/Pb zrn	Zartman & Richardson (2005)	[6]	-28.81110	27.42220
BOT17-03	K1	Orapa (Karowe, AK6 Pipe)	Botswana	93	3	U/Pb zrn	Tappe et al. (2018a)	[2]	-21.49560	25.47030
SAF18-51	K19	Jagersfontein	South Africa	95	5	U/Pb prv	Griffin et al. (2014)	[7]	-29.76230	25.41900
BOT17-01	K15	Orapa (Letlhakane, DK2 Pipe)	Botswana	106	4	U/Pb prv	Tappe et al. (2018a)	[2]	-21.52330	25.69610
ANG14-287	K6	Lunda Norte	Angola	123	4	U/Pb prv	Castillo-Oliver et al. (2016)	[8]	-8.07775	20.77671
BOT17-05	K2	Jwaneng (Pipe-8)	Botswana	235	4	U/Pb zrn	Kinny et al. (1989)	[9]	-24.65320	24.58010
ANG14-366	K17	Lubia	Angola	236	7	U/Pb zrn	Jelsma et al. (2013)	[10]	-11.01083	17.08760
SAF17-15	K10	Venetia (K4 Pipe)	South Africa	522	10	U/Pb prv	Griffin et al. (2014)	[7]	-22.43501	29.32903
PROTEROZOIC										
ITA-1	K14	Itanana	Tanzania	1083	11	U/Pb prv	Chesler (2012)	[11]	-4.18370	32.90370
CIM15-72	K4	Cullinan (Premier Pipe)	South Africa	1140	5	U/Pb prv	Tappe et al. (2018b)	[12]	-25.67360	28.51530
CIM15-80	K5	Cullinan (Premier Pipe)	South Africa	1140	5	U/Pb prv	Tappe et al. (2018b)	[12]	-25.67360	28.51530
SAF18-58	K30	Kuruman (Zero Pipe)	South Africa	1835	25	U/Pb prv	Donnelly et al. (2012)	[13]	-27.28217	23.72145
SAF18-59	K21	Kuruman (Zero Pipe)	South Africa	1835	25	U/Pb prv	Donnelly et al. (2012)	[13]	-27.28217	23.72145

[a]Decimal degrees geographic coordinates using WGS84 datum.

A sample locality map is provided in Figure S1 and the complete dataset is listed as Supplementary Data.

Abbreviations: bdl - baddeleyite; ol - olivine; phl - phlogopite; prv - perovskite; zrn - zircon.

Table S2: Tungsten isotopic compositions of magmatic Group-1 kimberlites from sub-Saharan Africa (sorted by emplacement age).

Sample ID	Run ID	Locality	Country	Age [Ma]	Weight [g]	Hf [µg/g]	W [µg/g]	Mo [µg/g]	n	$\mu^{182}W_{meas.}$ (± 2σ)	$\mu^{183}W_{meas.}$ (± 2σ)	$\mu^{183}W_{corr.}$ [a] (± 2σ)	$\mu^{182}W_{meas.}$ (± 2σ)	$\mu^{182}W_{corr.}$ [a] (± 2σ)	$\mu^{184}W_{meas.}$ (± 2σ)	$\mu^{184}W_{corr.}$ [a] (± 2σ)
										normalized to $^{186}W/^{184}W = 0.92767$			normalized to $^{186}W/^{183}W = 1.98590$			
MODERN																
IH17	K12	Igwisi Hills	Tanzania	0.012	0.55	4.68	2.37	0.47	10	-3.0 ± 2.7	-7.9 ± 2.6	-2.0 ± 3.9	7.7 ± 3.8	-2.6 ± 5.1	5.2 ± 1.7	1.3 ± 2.6
IH45	K28	Igwisi Hills	Tanzania	0.012	0.53	4.41	0.67	0.53	6	-2.8 ± 3.6	-12.8 ± 4.0	-2.0 ± 4.9	14.0 ± 3.7	-2.6 ± 6.4	8.5 ± 2.7	1.3 ± 3.3
IH53	K13	Igwisi Hills	Tanzania	0.012	0.55	3.26	0.68	0.29	7	-0.5 ± 3.4	-15.1 ± 3.7	-0.4 ± 5.2	19.1 ± 4.8	-0.6 ± 6.8	10.0 ± 2.5	0.3 ± 3.5
IH57	K7	Igwisi Hills	Tanzania	0.012	0.53	4.51	1.52	0.30	10	-6.0 ± 3.1	-14.3 ± 2.9	-4.3 ± 4.0	13.0 ± 3.7	-5.7 ± 5.2	9.5 ± 1.9	2.9 ± 2.7
IH57	K27	Igwisi Hills	Tanzania	0.012	0.52	n.a.	n.a.	n.a.	9	-0.8 ± 2.1	-7.3 ± 2.0	0.1 ± 2.5	9.6 ± 2.0	0.1 ± 3.2	4.8 ± 1.3	-0.1 ± 1.6
PHANEROZOIC																
ANG14-325	K16	Dando Kwanza	Angola	70	0.55	5.88	4.90	0.63	9	-1.0 ± 3.1	-5.0 ± 2.3	-0.2 ± 3.1	6.2 ± 2.8	-0.3 ± 4.1	3.3 ± 1.5	0.2 ± 2.1
NAM18-01	K29	Hanaus	Namibia	72	1.07	8.15	0.33	0.30	5	1.9 ± 5.1	-14.5 ± 4.9	1.8 ± 5.6	21.1 ± 3.6	2.2 ± 7.3	9.6 ± 3.2	-1.1 ± 3.7
NAM18-02	K18	Gibeon	Namibia	73	0.55	4.26	21.81	57.88	10	0.2 ± 2.7	-2.8 ± 2.3	0.2 ± 3.9	4.0 ± 4.1	0.3 ± 5.1	1.9 ± 1.5	-0.1 ± 2.6
BOT17-09	K3	Nxau-Nxau (K29 Pipe)	Botswana	84	0.51	6.38	0.69	0.10	7	-0.3 ± 3.3	-14.2 ± 2.9	0.5 ± 3.2	19.1 ± 1.7	0.5 ± 4.2	9.5 ± 2.0	-0.3 ± 2.1
LES17-01	K23	Letseng (Main Pipe)	Lesotho	85.5	1.07	4.50	0.50	0.30	8	0.9 ± 3.4	-13.3 ± 3.9	0.8 ± 5.6	18.4 ± 5.2	1.0 ± 7.3	8.9 ± 2.6	-0.5 ± 3.7
LES17-02	K8	Letseng (Main Pipe)	Lesotho	85.5	0.51	4.26	1.18	0.81	9	2.1 ± 3.0	-9.3 ± 3.4	1.3 ± 4.2	13.9 ± 3.3	1.7 ± 5.5	6.2 ± 2.2	-0.9 ± 2.8
LES17-02	K11	Letseng (Main Pipe)	Lesotho	85.5	1.50	n.a.	n.a.	n.a.	9	-1.4 ± 3.2	-10.9 ± 3.4	-0.7 ± 4.1	13.2 ± 3.1	-1.0 ± 5.4	7.3 ± 2.2	0.5 ± 2.8
LES17-02	K22	Letseng (Main Pipe)	Lesotho	85.5	1.06	n.a.	n.a.	n.a.	10	0.2 ± 3.9	-10.0 ± 3.4	0.3 ± 4.6	13.4 ± 4.0	0.3 ± 6.0	6.7 ± 2.3	-0.2 ± 3.1
LES17-03	K24	Letseng (Main Pipe)	Lesotho	85.5	1.07	3.99	0.79	0.20	9	0.7 ± 2.9	-14.2 ± 3.4	0.7 ± 4.0	19.4 ± 2.8	0.8 ± 5.2	9.5 ± 2.2	-0.4 ± 2.7
SAF17-11	K9	Kimberley (De Beers Pipe)	South Africa	87	0.51	6.36	0.91	0.43	8	0.0 ± 4.7	-11.7 ± 3.1	0.3 ± 3.9	15.5 ± 3.1	0.3 ± 5.1	7.8 ± 2.1	-0.2 ± 2.6
SAF18-57	K20	Monastery	South Africa	89.8	0.57	12.98	0.44	7.39	4	-0.7 ± 4.8	-16.8 ± 5.0	0.6 ± 8.4	22.7 ± 8.8	0.7 ± 10.9	11.2 ± 3.3	-0.4 ± 5.6
BOT17-03	K1	Orapa (Karowe, AK6 Pipe)	Botswana	93	0.53	3.18	0.27	0.12	2	3.9 ± 8.6	-11.1 ± 9.0	3.2 ± 11.3	18.5 ± 8.8	4.1 ± 14.7	7.4 ± 6.0	-2.1 ± 7.5
SAF18-51	K19	Jagersfontein	South Africa	95	0.55	9.38	7.99	0.52	10	-3.0 ± 2.2	-4.3 ± 3.2	-1.9 ± 4.5	3.2 ± 4.1	-2.5 ± 5.8	2.9 ± 2.1	1.3 ± 3.0
BOT17-01	K15	Orapa (Letlhakane, DK2 Pipe)	Botswana	106	0.55	5.01	0.45	0.17	4	0.1 ± 8.6	-15.6 ± 6.7	0.7 ± 9.5	21.1 ± 8.8	0.8 ± 12.3	10.3 ± 4.4	-0.4 ± 6.3
ANG14-287	K6	Lunda Norte	Angola	123	0.55	9.11	2.15	3.44	10	0.4 ± 1.3	-11.3 ± 2.6	0.3 ± 3.9	15.1 ± 3.8	0.4 ± 5.0	7.5 ± 1.7	-0.2 ± 2.6
ANG14-287	K25	Lunda Norte	Angola	123	0.50	n.a.	n.a.	n.a.	10	2.2 ± 3.0	-8.3 ± 2.6	2.3 ± 4.1	13.7 ± 4.1	2.9 ± 5.3	5.5 ± 1.7	-1.5 ± 2.7
BOT17-05	K2	Jwaneng (Pipe-8)	Botswana	235	0.51	2.36	0.16	0.29	1	0.2 ± 8.6	-13.3 ± 9.0	0.7 ± 11.3	18.2 ± 8.8	0.8 ± 14.7	8.8 ± 6.0	-0.4 ± 7.5
ANG14-366	K17	Lubia	Angola	236	0.57	3.27	0.37	0.23	4	-3.6 ± 7.8	-20.2 ± 5.3	-2.5 ± 5.3	23.0 ± 1.1	-3.3 ± 7.0	13.4 ± 3.5	1.7 ± 3.6
SAF17-15	K10	Venetia (K4 Pipe)	South Africa	522	0.53	1.98	2.97	1.37	10	0.6 ± 3.6	-7.2 ± 4.5	0.7 ± 5.3	10.4 ± 3.7	0.9 ± 6.9	4.8 ± 3.0	-0.5 ± 3.5
SAF17-15	K26	Venetia (K4 Pipe)	South Africa	522	0.52	n.a.	n.a.	n.a.	9	1.9 ± 2.8	-3.5 ± 2.3	1.9 ± 3.0	7.0 ± 2.5	2.4 ± 3.9	2.3 ± 1.5	-1.2 ± 2.0
PROTEROZOIC																
ITA-1	K14	Itanana	Tanzania	1083	0.56	9.34	2.54	4.43	10	-2.1 ± 3.1	-8.0 ± 2.9	-1.6 ± 3.8	8.3 ± 3.3	-2.2 ± 5.0	5.3 ± 1.9	1.1 ± 2.6
CIM15-72	K4	Cullinan (Premier Pipe)	South Africa	1140	0.52	1.85	0.54	0.29	5	1.2 ± 5.3	-12.0 ± 4.8	1.6 ± 7.3	17.7 ± 7.3	2.0 ± 9.6	8.0 ± 3.2	-1.0 ± 4.9
CIM15-80	K5	Cullinan (Premier Pipe)	South Africa	1140	0.52	2.11	0.53	0.29	5	0.3 ± 6.1	-13.4 ± 4.5	1.0 ± 7.3	18.7 ± 7.5	1.3 ± 9.5	8.9 ± 3.0	-0.6 ± 4.9
SAF18-58	K30	Kuruman (Zero Pipe)	South Africa	1835	0.52	4.50	2.97	1.23	10	1.8 ± 3.8	-7.4 ± 3.0	1.8 ± 3.4	11.9 ± 2.1	2.3 ± 4.5	4.9 ± 2.0	-1.2 ± 2.3
SAF18-59	K21	Kuruman (Zero Pipe)	South Africa	1835	0.57	5.94	2.16	0.37	10	4.0 ± 2.6	-7.5 ± 1.9	3.4 ± 3.4	14.1 ± 3.6	4.4 ± 4.4	5.0 ± 1.3	-2.2 ± 2.2

n = number of multiple W isotope ratio measurements of the same sample solution to obtain a mean of pooled solution replicates.
The Hf and W concentrations were determined by ID-MC-ICPMS and the Mo concentrations by Q-ICPMS (see Methods).
n.a. = not analyzed.

[a]Corrected for a small analytical effect on ^{183}W (see Table S4); reported uncertainties entail all propagated errors that were introduced by this ^{183}W correction.
Reported uncertainties of the measured µW values represent either the external reproducibility (2SD) obtained by repeated analyses of the JB-2 standard (Table S4), or 95% Confidence Intervals for samples with >3 replicate measurements of the solutions (n>3).

Table S3: Summary of average tungsten isotopic compositions of magmatic Group-1 kimberlites from 18 individual occurrences across Africa (sorted by emplacement age).

Locality	Country	Age [Ma]	Latitude	Longitude	n	$\mu^{182}W_{meas.}$ (± 2SD)	$\mu^{183}W_{corr.}$ [a] (± 2SD)	$\mu^{182}W_{corr.}$ [a] (± 2SD)	$\mu^{184}W_{corr.}$ [a] (± 2SD)
						normalized to $^{186}W/^{184}W = 0.92767$		normalized to $^{186}W/^{183}W = 1.98590$	
MODERN									
Igwisi Hills	Tanzania	0.012	-4.86670	31.91670	5	**-2.6 ± 4.4**	-1.7 ± 3.5	-2.3 ± 4.5	1.2 ± 2.3
PHANEROZOIC									
Dando Kwanza	Angola	70	-11.35651	17.01033	1	**-1.0 ± 3.1**	-0.2 ± 3.1	-0.3 ± 4.1	0.2 ± 2.1
Hanaus	Namibia	72	-25.23920	17.70890	1	**1.9 ± 5.1**	1.8 ± 5.6	2.2 ± 7.3	-1.1 ± 3.7
Gibeon	Namibia	73	-24.99310	17.80110	1	**0.2 ± 2.7**	0.2 ± 3.9	0.3 ± 5.1	-0.1 ± 2.6
Nxau-Nxau (K29 Pipe)	Botswana	84	-18.94705	21.14181	1	**-0.3 ± 3.3**	0.5 ± 3.2	0.5 ± 4.2	-0.3 ± 2.1
Letseng (Main Pipe)	Lesotho	85	-29.00600	28.86700	5	**0.5 ± 2.5**	0.5 ± 1.5	0.6 ± 2.0	-0.3 ± 1.0
Kimberley (De Beers Pipe)	South Africa	87	-28.73890	24.77640	1	**0.0 ± 4.7**	0.3 ± 3.9	0.3 ± 5.1	-0.2 ± 2.6
Monastery	South Africa	90	-28.81110	27.42220	1	**-0.7 ± 4.8**	0.6 ± 8.4	0.7 ± 10.9	-0.4 ± 5.6
Orapa (Karowe, AK6 Pipe)	Botswana	93	-21.49560	25.47030	1	**3.9 ± 8.6**	3.2 ± 11.3	4.1 ± 14.7	-2.1 ± 7.5
Jagersfontein	South Africa	95	-29.76230	25.41900	1	**-3.0 ± 2.2**	-1.9 ± 4.5	-2.5 ± 5.8	1.3 ± 3.0
Orapa (Letlhakane, DK2 Pipe)	Botswana	106	-21.52330	25.69610	1	**0.1 ± 8.6**	0.7 ± 9.5	0.8 ± 12.3	-0.4 ± 6.3
Lunda Norte	Angola	123	-8.07775	20.77671	2	**1.3 ± 2.6**	1.3 ± 2.7	1.7 ± 3.6	-0.9 ± 1.8
Jwaneng (Pipe-8)	Botswana	235	-24.65320	24.58010	1	**0.2 ± 8.6**	0.7 ± 11.3	0.8 ± 14.7	-0.4 ± 7.5
Lubia	Angola	236	-11.01083	17.08760	1	**-3.6 ± 7.8**	-2.5 ± 5.3	-3.3 ± 7.0	1.7 ± 3.6
Venetia (K4 Pipe)	South Africa	522	-22.43501	29.32903	2	**1.2 ± 1.8**	1.3 ± 1.6	1.7 ± 2.1	-0.9 ± 1.1
PROTEROZOIC									
Itanana	Tanzania	1083	-4.18370	32.90370	1	**-2.1 ± 3.1**	-1.6 ± 3.8	-2.2 ± 5.0	1.1 ± 2.6
Cullinan (Premier Pipe)	South Africa	1153	-25.67360	28.51530	2	**0.7 ± 1.2**	1.3 ± 0.8	1.6 ± 1.1	-0.8 ± 0.5
Kuruman (Zero Pipe)	South Africa	1835	-27.28217	23.72145	2	**2.9 ± 3.1**	2.6 ± 2.3	3.3 ± 3.0	-1.7 ± 1.5
Mean average for African kimberlites (this study):						***-0.02 ± 3.94***			

n = number of individual samples and/or replicate sample digests included into the calculation of the mean average W isotopic composition for each listed kimberlite locality (for samples with n>1, the uncertainties on average $\mu^{i}W$ values represent the 2SD of the individual samples/digestions).
See Table S2 for the complete W isotope dataset.
Geographic coordinates are in decimal degrees using WGS84 datum.

[a]Corrected for a small analytical effect on ^{183}W (see Table S4); reported uncertainties entail all propagated errors that were introduced by this ^{183}W correction.

Table S4: Tungsten isotopic compositions of geological reference materials analyzed during the course of this study.

Sample ID	Hf [µg/g]	W [µg/g]	$\mu^{182}W_{meas.}$ (± 2SE)	$\mu^{183}W_{meas.}$ (± 2SE)	$\mu^{183}W_{corr.}$ [a] (± 2σ)	$\mu^{182}W_{meas.}$ (± 2SE)	$\mu^{182}W_{corr.}$ [a] (± 2σ)	$\mu^{184}W_{meas.}$ (± 2SE)	$\mu^{184}W_{corr.}$ [a] (± 2σ)
			normalized to $^{186}W/^{184}W = 0.92767$			normalized to $^{186}W/^{183}W = 1.98590$			
JB-2 (arc basalt)									
JB202.1	1.49	0.32	0.0 ± 8.7	-18.7 ± 7.8	0.4 ± 9.8	24.8 ± 7.6	0.5 ± 12.7	12.4 ± 5.2	-0.2 ± 6.5
JB202.2	–	–	3.9 ± 8.3	-15.3 ± 8.0	3.4 ± 10.3	24.3 ± 8.4	4.4 ± 13.4	10.2 ± 5.3	-2.2 ± 6.8
JB202.3	–	–	4.6 ± 8.8	-19.0 ± 7.8	4.0 ± 9.8	29.9 ± 7.7	5.1 ± 12.7	12.7 ± 5.2	-2.6 ± 6.5
JB204.1	1.49	0.31	-5.8 ± 7.5	-27.1 ± 6.6	-3.6 ± 8.3	30.6 ± 6.6	-4.7 ± 10.8	18.0 ± 4.4	2.4 ± 5.5
JB204.2	–	–	4.3 ± 7.1	-12.6 ± 7.2	4.1 ± 9.4	21.7 ± 7.7	5.3 ± 12.2	8.4 ± 4.8	-2.7 ± 6.2
JB204.3	–	–	-4.2 ± 8.0	-23.4 ± 7.1	-2.7 ± 9.1	27.0 ± 7.3	-3.6 ± 11.8	15.6 ± 4.7	1.8 ± 6.0
JB205.1	1.55	0.32	1.9 ± 7.4	-14.2 ± 6.4	1.8 ± 8.1	20.8 ± 6.4	2.3 ± 10.5	9.4 ± 4.3	-1.2 ± 5.4
JB205.2	–	–	-4.8 ± 7.6	-17.0 ± 6.7	-3.2 ± 8.3	17.9 ± 6.3	-4.2 ± 10.8	11.3 ± 4.5	2.2 ± 5.5
JB205.3	–	–	4.3 ± 6.9	-18.5 ± 6.1	3.8 ± 8.1	29.0 ± 6.8	4.9 ± 10.5	12.3 ± 4.1	-2.5 ± 5.4
n	3	3	9	9	9	9	9	9	9
Mean	1.51	0.31	0.5	-18.4	0.9	25.1	1.1	12.2	-0.6
2S.D.	0.07	0.01	8.6	9.0	6.5	8.8	8.5	6.0	4.3
95% C.I.	0.09	0.01	3.3	3.5	2.5	3.4	3.3	2.3	1.7
JG-1 (granodiorite)									
DI35.50	–	–	-2.8 ± 6.7	-9.7 ± 6.0	-1.9 ± 7.7	10.1 ± 6.2	-2.8 ± 10.0	6.5 ± 4.0	1.4 ± 5.1
DI35.51	–	–	3.9 ± 6.9	-1.5 ± 5.6	2.9 ± 7.5	5.7 ± 6.5	3.8 ± 9.8	1.0 ± 3.7	-1.9 ± 5.0
DI35.52	–	–	3.8 ± 7.5	4.6 ± 6.1	2.7 ± 8.0	-2.4 ± 6.7	3.6 ± 10.5	-3.1 ± 4.1	-1.8 ± 5.3
DI35.53	–	–	0.8 ± 6.6	-1.6 ± 6.0	1.8 ± 7.8	4.3 ± 6.5	2.3 ± 10.1	1.0 ± 4.0	-1.2 ± 5.2
DI35.54	–	–	-0.4 ± 7.0	-6.0 ± 6.1	-0.3 ± 8.2	7.4 ± 7.1	-0.4 ± 10.7	4.0 ± 4.1	0.2 ± 5.5
DI35.55	–	–	6.6 ± 6.9	-1.3 ± 6.0	4.5 ± 7.6	7.5 ± 5.9	5.8 ± 9.9	0.9 ± 4.0	-3.0 ± 5.0
DI35.56	–	–	-4.7 ± 7.1	-9.4 ± 6.3	-2.3 ± 8.1	9.2 ± 6.6	-3.1 ± 10.5	6.2 ± 4.2	1.6 ± 5.4
DI35.57	–	–	8.6 ± 6.4	-0.5 ± 6.0	6.9 ± 7.7	9.5 ± 6.2	8.9 ± 10.1	0.3 ± 4.0	-4.5 ± 5.1
DI35.58	–	–	-5.9 ± 7.2	-5.9 ± 6.5	-4.3 ± 8.4	2.0 ± 6.9	-5.6 ± 10.9	3.9 ± 4.3	2.9 ± 5.6
DI35.59	–	–	-8.9 ± 7.3	-3.2 ± 6.7	-6.1 ± 8.4	-3.7 ± 6.5	-7.9 ± 10.9	2.1 ± 4.5	4.0 ± 5.6
n	–	–	10	10	10	10	10	10	10
Mean	–	–	0.1	-3.4	0.4	5.0	0.5	2.3	-0.2
2S.D.	–	–	11.4	8.7	8.1	9.8	10.6	5.8	5.4
95% C.I.	–	–	4.1	3.1	2.9	3.5	3.8	2.1	1.9
JA-2 (andesite)									
DI36.50	–	–	-0.8 ± 7.0	-12.1 ± 6.3	0.7 ± 8.3	16.6 ± 7.1	0.5 ± 10.9	8.2 ± 4.2	-0.3 ± 5.5
DI36.51	–	–	6.4 ± 8.0	-0.4 ± 6.3	6.3 ± 8.2	8.7 ± 6.8	8.2 ± 10.7	0.3 ± 4.2	-4.2 ± 5.5
DI36.52	–	–	0.1 ± 5.9	-3.7 ± 5.3	0.4 ± 6.9	5.4 ± 5.7	0.6 ± 9.0	2.5 ± 3.5	-0.3 ± 4.6
DI36.53	–	–	8.2 ± 6.4	2.4 ± 5.6	7.3 ± 7.1	6.3 ± 5.7	9.5 ± 9.2	-1.6 ± 3.7	-4.8 ± 4.7
DI36.54	–	–	-1.9 ± 5.7	-9.3 ± 5.2	-0.2 ± 7.0	11.7 ± 6.2	-0.3 ± 9.1	6.2 ± 3.4	0.2 ± 4.7
DI36.55	–	–	-2.8 ± 6.7	-1.1 ± 6.5	-2.5 ± 8.8	-1.9 ± 7.7	-3.3 ± 11.5	0.7 ± 4.3	1.7 ± 5.9
DI36.56	–	–	11.0 ± 6.6	-1.3 ± 5.7	8.7 ± 7.3	13.0 ± 6.1	11.3 ± 9.6	0.9 ± 3.8	-5.8 ± 4.9
DI36.57	–	–	-1.6 ± 6.9	-9.0 ± 5.9	-0.5 ± 7.9	11.0 ± 6.9	-0.7 ± 10.3	6.0 ± 3.9	0.4 ± 5.3
DI36.58	–	–	-3.0 ± 6.9	-2.1 ± 6.4	-1.6 ± 8.2	0.6 ± 6.7	-2.1 ± 10.7	1.4 ± 4.2	1.1 ± 5.5
DI36.59	–	–	-1.2 ± 6.5	-3.9 ± 5.7	-1.1 ± 7.0	3.7 ± 5.3	-1.4 ± 9.2	2.6 ± 3.8	0.7 ± 4.7
n	–	–	10	10	10	10	10	10	10
Mean	–	–	1.4	-4.0	1.7	7.5	2.2	2.7	-1.1
2S.D.	–	–	10.2	9.2	8.2	11.6	10.6	6.2	5.4
95% C.I.	–	–	3.6	3.3	2.9	4.1	3.8	2.2	1.9

The Hf and W concentrations were determined by ID-MC-ICPMS (see Methods).
C.I. = Confidence Interval.

The rock standards were processed through the full chemical separation procedure and analyzed with each set of samples.
JG-1 and JA-2 were digested once (1.0–1.5 g); JB-2 was digested three times (0.5 g per digestion).
Each reported line represents a single measurement, which consumed about 40 ng of W (run at 50 ppb).

[a]Corrected for a small analytical effect on ^{183}W according to (*i*) $\varepsilon^{183}W\ (6/4)_{corr.} = \varepsilon^{183}W\ (6/4)_{meas.} + 0.769 \times \varepsilon^{182}W\ (6/3)_{meas.}$,
(*ii*) $\varepsilon^{182}W\ (6/3)_{corr.} = \varepsilon^{182}W\ (6/3)_{meas.} - 1.962 \times \varepsilon^{184}W\ (6/3)_{meas.}$, and (*iii*) $\varepsilon^{184}W\ (6/3)_{corr.} = \varepsilon^{184}W\ (6/3)_{meas.} - 0.510 \times \varepsilon^{182}W\ (6/3)_{meas.}$ (ref. 68 in Methods).

Uncertainties on corrected $\mu^{i}W$ values include all propagated uncertainties induced by the ^{183}W correction.

References in Supplementary file C

1 Brown, R. J. *et al.* Eruption of kimberlite magmas: Physical volcanology, geomorphology and age of the youngest kimberlitic volcanoes known on Earth (the Upper Pleistocene/Holocene Igwisi Hills volcanoes, Tanzania). *Bull. Volcanol.* **74**, 1621-1643 (2012).

2 Tappe, S., Smart, K. A., Torsvik, T. H., Massuyeau, M. & de Wit, M. C. J. Geodynamics of kimberlites on a cooling Earth: Clues to plate tectonic evolution and deep volatile cycles. *Earth and Planetary Science Letters* **484**, 1-14 (2018).

3 Farr, H., Phillips, D., Maas, R. & de Wit, M. C. J. Petrography, Sr-isotope geochemistry and geochronology of the Nxau Nxau kimberlites, north-west Botswana. *Mineral. Petrol.* **112**, 625-638 (2018).

4 Stamm, N. *et al.* Primary petrology, mineralogy and age of the Letšeng-la-Terae kimberlite (Lesotho, Southern Africa) and parental magmas of Group-I kimberlites. *Contrib. Mineral. Petrol.* **173**, 1-25 (2018).

5 Batumike, J. M. *et al.* LAM-ICPMS U-Pb dating of kimberlitic perovskite: Eocene-Oligocene kimberlites from the Kundelungu Plateau, D.R. Congo. *Earth and Planetary Science Letters* **267**, 609-619 (2008).

6 Zartman, R. E. & Richardson, S. H. Evidence from kimberlitic zircon for a decreasing mantle Th/ U since the Archean. *Chemical Geology* **220**, 263-283 (2005).

7 Griffin, W. L. *et al.* Emplacement ages and sources of kimberlites and related rocks in southern Africa: U-Pb ages and Sr-Nd isotopes of groundmass perovskite. *Contrib. Mineral. Petrol.* **168**, 1-13 (2014).

8 Castillo-Oliver, M. *et al.* Trace-element geochemistry and U-Pb dating of perovskite in kimberlites of the Lunda Norte province (NE Angola): Petrogenetic and tectonic implications. *Chemical Geology* **426**, 118-134, doi:pdf (2016).

9 Kinny, P. D., Compston, W., Bristow, J. W. & Williams, I. S. in *Kimberlites and related rocks* Vol. 14 (ed J. Ross) 833-842 (Geol. Soc. Australia Spec. Publ., 1989).

10 Jelsma, H. *et al.* in *Proceedings of the 10th International Kimberlite Conference* (ed D.G. Pearson) 173-190 (Springer, 2013).

11 Chesler, R. *The geochemistry and geochronology of Tanzanian kimberlites* Ph.D. thesis, The University of Melbourne, (2012).

12 Tappe, S., Dongre, A., Liu, C.-Z. & Wu, F.-Y. 'Premier' evidence for prolonged kimberlite pipe formation and its influence on diamond transport from deep Earth. *Geology* **46**, 843–846, doi:10.1130/G45097.1 (2018).

13 Donnelly, C. L. *et al.* In situ U-Pb dating and Sr-Nd isotopic analysis of perovskite: Constraints on the age and petrogenesis of the Kuruman kimberlite province, Kaapvaal craton, South Africa. *J. Petrol.* **53**, 2497-2522 (2012).

14 Harte, B. & Richardson, S. H. Mineral inclusions in diamonds track the evolution of a Mesozoic subducted slab beneath West Gondwanaland. *Gondwana Res.* **21**, 236-245 (2012).

15 Smith, E. M. *et al.* Blue boron-bearing diamonds from Earth's lower mantle. *Nature* **560**, 84-87 (2018).

16 Smith, E. M. *et al.* Large gem diamonds from metallic liquid in Earth's deep mantle. *Science* **354**, 1403-1405 (2016).

17 Nestola, F. *et al.* $CaSiO_3$ perovskite in diamond indicates the recycling of oceanic crust into the lower mantle. *Nature* **555**, 237-241 (2018).

18 Tappert, R. *et al.* Diamonds from Jagersfontein (South Africa): Messengers from the sublithospheric mantle. *Contrib. Mineral. Petrol.* **150**, 505-522 (2005).
19 Motsamai, T., Harris, J. W., Stachel, T., Pearson, D. G. & Armstrong, J. Mineral inclusions in diamonds from Karowe Mine, Botswana: Super-deep sources for super-sized diamonds? *Mineral. Petrol.* **112**, 169-180 (2018).
20 Moore, R. O. & Gurney, J. J. Pyroxene solid solution in garnets included in diamond. *Nature* **318**, 553-555 (1985).
21 Schersten, A., Elliott, T., Hawkesworth, C. & Norman, M. Tungsten isotope evidence that mantle plumes contain no contribution from the Earth's core. *Nature* **427**, 234-237 (2004).
22 Clement, C. R. *A comparative geological study of some major kimberlite pipes in the Northern Cape and Orange Free State* Ph.D. thesis, University of Cape Town, (1982).
23 le Roex, A. P., Bell, D. R. & Davis, P. Petrogenesis of Group I kimberlites from Kimberley, South Africa: Evidence from bulk-rock geochemistry. *J. Petrol.* **44**, 2261-2286 (2003).
24 Kjarsgaard, B. A., Pearson, D. G., Tappe, S., Nowell, G. M. & Dowall, D. Geochemistry of hypabyssal kimberlites from Lac de Gras, Canada: Comparisons to a global database and applications to the parent magma problem. *Lithos* **112**, 236-248 (2009).
25 Tappe, S. *et al.* Sources and mobility of carbonate melts beneath cratons, with implications for deep carbon cycling, metasomatism and rift initiation. *Earth and Planetary Science Letters* **466**, 152-167 (2017).
26 Willbold, M. & Stracke, A. Trace element composition of mantle end-members: Implications for recycling of oceanic and upper and lower continental crust. *Geochemistry Geophysics Geosystems* **7**, Q04004 (2006).
27 Becker, M. & le Roex, A. P. Geochemistry of South African on- and off-craton, Group I and Group II kimberlites: Petrogenesis and source region evolution. *J. Petrol.* **47**, 673-703 (2006).
28 Coe, N., le Roex, A. P., Gurney, J. J., Pearson, D. G. & Nowell, G. M. Petrogenesis of the Swartruggens and Star Group II kimberlite dyke swarms, South Africa: Constraints from whole rock geochemistry. *Contrib. Mineral. Petrol.* **156**, 627-652 (2008).
29 le Roex, A. P. Geochemical correlation between southern African kimberlites and South Atlantic hotspots. *Nature* **324**, 243-245 (1986).
30 Palme, H. & O'Neill, H. S. C. in *Treatise on Geochemistry* Vol. 2 (ed R.W. Carlson) 1-38 (Elsevier, 2003).
31 Arevalo, R. & McDonough, W. F. Tungsten geochemistry and implications for understanding the Earth's interior. *Earth and Planetary Science Letters* **272**, 656-665 (2008).
32 Touboul, M., Puchtel, I. S. & Walker, R. J. W-182 evidence for long-term preservation of early mantle differentiation products. *Science* **335**, 1065-1069 (2012).
33 Puchtel, I. S., Blichert-Toft, J., Touboul, M., Horan, M. F. & Walker, R. J. The coupled W-182-Nd-142 record of early terrestrial mantle differentiation. *Geochemistry Geophysics Geosystems* **17**, 2168-2193 (2016).
34 König, S., Münker, C., Schuth, S. & Garbe-Schönberg, D. Mobility of tungsten in subduction zones. *Earth and Planetary Science Letters* **274**, 82-92 (2008).
35 König, S. *et al.* Boninites as windows into trace element mobility in subduction zones. *Geochim. Cosmochim. Acta* **74**, 684-704 (2010).
36 König, S. *et al.* The Earth's tungsten budget during mantle melting and crust formation. *Geochim. Cosmochim. Acta* **75**, 2119-2136 (2011).

37 Liu, J. G., Pearson, D. G., Chacko, T. & Luo, Y. A reconnaissance view of tungsten reservoirs in some crustal and mantle rocks: Implications for interpreting W isotopic compositions and crust-mantle W cycling. *Geochim. Cosmochim. Acta* **223**, 300-318 (2018).
38 Mundl, A., Walker, R. J., Reimink, J. R., Rudnick, R. L. & Gaschnig, R. M. Tungsten-182 in the upper continental crust: Evidence from glacial diamictites. *Chemical Geology* **494**, 144-152 (2018).
39 Brey, G. P., Bulatov, V. K., Girnis, A. V. & Lahaye, Y. Experimental melting of carbonated peridotite at 6-10 GPa. *J. Petrol.* **49**, 797-821 (2008).
40 Dasgupta, R., Hirschmann, M. M., McDonough, W. F., Spiegelman, M. & Withers, A. C. Trace element partitioning between garnet lherzolite and carbonatite at 6.6 and 8.6 GPa with applications to the geochemistry of the mantle and of mantle-derived melts. *Chemical Geology* **262**, 57-77 (2009).
41 Chauvel, C., Lewin, E., Carpentier, M., Arndt, N. T. & Marini, J. C. Role of recycled oceanic basalt and sediment in generating the Hf-Nd mantle array. *Nat. Geosci.* **1**, 64-67 (2008).
42 Nowell, G. M. *et al.* Hf isotope systematics of kimberlites and their megacrysts: New constraints on their source regions. *J. Petrol.* **45**, 1583-1612 (2004).
43 Gaffney, A. M. *et al.* Constraints on source-forming processes of West Greenland kimberlites inferred from Hf-Nd isotope systematics. *Geochim. Cosmochim. Acta* **71**, 2820-2836 (2007).
44 Tappe, S. *et al.* A fresh isotopic look at Greenland kimberlites: Cratonic mantle lithosphere imprint on deep source signal. *Earth and Planetary Science Letters* **305**, 235-248 (2011).
45 Tappe, S., Pearson, D. G., Kjarsgaard, B. A., Nowell, G. M. & Dowall, D. Mantle transition zone input to kimberlite magmatism near a subduction zone: Origin of anomalous Nd-Hf isotope systematics at Lac de Gras, Canada. *Earth and Planetary Science Letters* **371-372**, 235-251, doi:pdf (2013).
46 Tappe, S., Kjarsgaard, B. A., Kurszlaukis, S., Nowell, G. M. & Phillips, D. Petrology and Nd-Hf isotope geochemistry of the Neoproterozoic Amon kimberlite sills, Baffin Island (Canada): Evidence for deep mantle magmatic activity linked to supercontinent cycles. *J. Petrol.* **55**, 2003-2042 (2014).
47 Tappe, S. *et al.* Plates or plumes in the origin of kimberlites: U/Pb perovskite and Sr-Nd-Hf-Os-C-O isotope constraints from the Superior craton (Canada). *Chemical Geology* **455**, 57-83, doi:10.1016/j.chemgeo.2016.08.019 (2017).
48 Carlson, R. W., Czamanske, G., Fedorenko, V. & Ilupin, I. A comparison of Siberian meimechites and kimberlites: Implications for the source of high-Mg alkalic magmas and flood basalts. *Geochemistry Geophysics Geosystems* **7**, Q11014 (2006).
49 Paton, C., Hergt, J. M., Woodhead, J. D., Phillips, D. & Shee, S. R. Identifying the asthenospheric component of kimberlite magmas from the Dharwar craton, India. *Lithos* **112**, 296-310 (2009).
50 Yaxley, G. M. *et al.* The discovery of kimberlites in Antarctica extends the vast Gondwanan Cretaceous province. *Nat. Commun.* **4**, 1-7 (2013).
51 Smith, C. B. Pb, Sr and Nd isotopic evidence for sources of southern African Cretaceous kimberlites. *Nature* **304**, 51-54 (1983).
52 Sarkar, C., Storey, C. D. & Hawkesworth, C. J. Using perovskite to determine the pre-shallow level contamination magma characteristics of kimberlite. *Chemical Geology* **363**, 76-90 (2014).